analytical chemistry

Deterministic Lateral Displacement Using Hexagonally Arranged, Bottom-Up-Inspired Micropost Arrays

Talha M. Razaulla, Olivia M. Young, Abdullah Alsharhan, Ryan D. Sochol, and Roseanne Warren*

Cite This: *Anal. Chem.* 2022, 94, 1949−1957

Read Online

ABSTRACT: Size-based separation of particles in microfluidic devices can be achieved using arrays of micro- or nanoscale posts using a technique known as deterministic lateral displacement (DLD). To date, DLD arrays have been limited to parallelogram or rotated-square arrangements of posts, with various post shapes having been explored in these two principal arrangements. This work examines a new DLD geometry based on patterning obtainable through self-assembly of single-layer nanospheres, which we call hexagonally arranged triangle (HAT) geometry. Finite element simulations are used to characterize the DLD separation properties of the HAT geometry. The relationship between the array angle, the gap spacing, and the critical diameter for separation is derived for the HAT geometry and expressed in a similar mathematical form as conventional parallelogram and rotated-square DLD arrays. At array angles <7°, HAT structures demonstrate smaller particle sorting capability (smaller critical diameter-to-gap spacing ratio) compared to published experimental results for parallelogram-type DLD arrays with circular posts. Experimental validation of DLD separation confirms the separation ability of the HAT array geometry. It is envisioned that this work will provide the first step toward future implementation of nanoscale DLD arrays fabricated by low-cost, bottom-up self-assembly approaches.

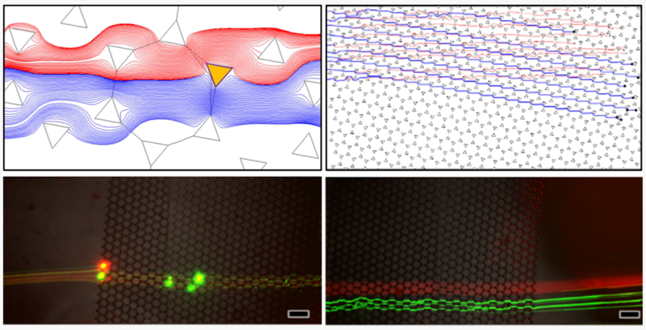

The separation of particles based on size is a useful technique in many fields, including laboratory-on-a-chip applications such as cellular analysis, diagnostics, and therapeutics.[1,2] Deterministic lateral displacement (DLD) is a microfluidic separation technique in which particles in a flow stream pass through a carefully designed array of micro- or nanoscale posts (Figure 1a).[3] Separation is achieved based on differences in laminar flow streams traveled by particles larger or smaller than a given critical diameter (Figure 1b). Particles larger than the critical diameter move through the channel in "bumping" mode, thereby undergoing lateral displacement. Particles smaller than the critical diameter move in a "zig-zag" path around the posts, thereby undergoing net zero lateral displacement. More complex mixed-motion phenomena (e.g., alternating bumping and zig-zag path) have also been observed with some DLD post geometries and shapes.[4−6] In contrast to active particle separation techniques requiring external forces (e.g., acoustic, electric, or gravitational[7−10]), DLD passively separates particles, thus providing a gentle, "label-free" approach to particle manipulation.[11] Additional advantages of DLD compared to other separation techniques include: (1) clog-free separation, as the critical particle size is less than the post gap spacing;[12] (2) continuous separation with the potential for real-time tuning of separation ranges;[13] and (3) robustness to array defects because of the repetitive separation action.[14]

Since its demonstration in 2004, DLD separation has proven effective for rigid and deformable particles, as well as nonspherical particles such as red blood cells[15,16] and rod-shaped bacteria.[16] Applications of DLD include leukocyte enrichment,[17,18] separation of parasites from human blood,[19,20] label-free measurement of platelet activation;[21] cell enrichment for tissue engineering;[22] cell lysis and labeling;[23] size-based droplet separation;[24,25] as well as circulating tumor cell (CTC) isolation and enrichment.[26,27] More recently, there is growing interest in nanoscale DLD ("nanoDLD") for purifying submicron particles, including extracellular vesicles (EVs),[28−30] colloids, and biopolymers. Wunsch et al. demonstrated DLD-based purification of 20 nm spherical particles using DLD nanopost arrays with 42 nm gap spacing fabricated by electron-beam lithography (EBL).[29] The researchers further demonstrated separation of exosomes with diameters ranging from 20 to 140 nm using nanoDLD arrays,[29] as well as double-stranded DNA concentration and

Received: July 19, 2021
Accepted: January 3, 2022
Published: January 18, 2022

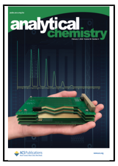

https://doi.org/10.1021/acs.analchem.1c03035
Anal. Chem. 2022, 94, 1949−1957

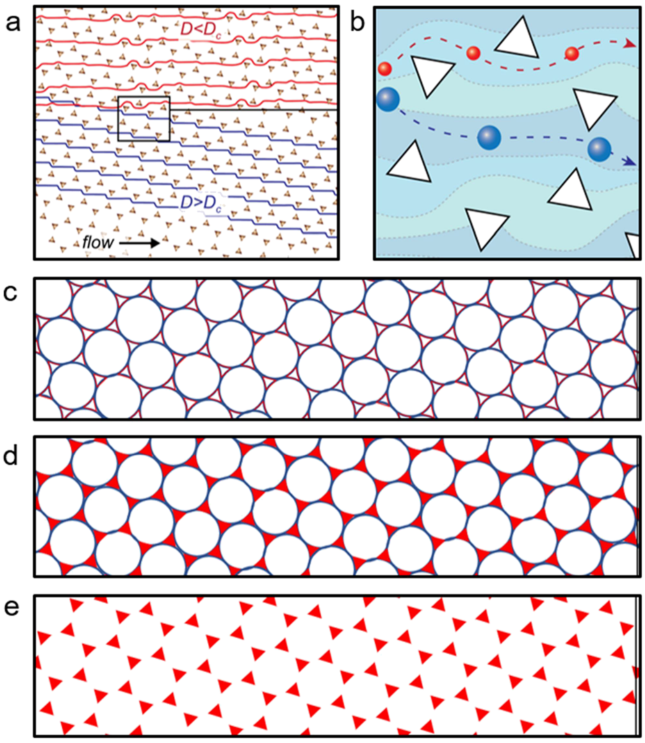

Figure 1. Conceptual illustration of HAT DLD array particle separation and pattern generation. (a) Particle trajectories for rigid spherical particles with diameter (D) greater than (blue) and less than (red) the critical diameter (D_c). (b) Zoomed-in view illustrating size-based separation through streamlines. (c) Single-layer NSL templating spheres arranged in hexagonal packing. (d) Interstitial gaps between spheres filled through a deposition process. (e) Templating spheres removed through lift-off, leading to the formation of the HAT pattern.

separation.[31] To date, nanoDLD arrays with gap spacings of 25−750 nm have mostly been fabricated using EBL.[29,31,32] While EBL produces highly accurate pattern replication at the nanoscale, the pixel-by-pixel exposure approach of EBL results in slow, costly fabrication of nanoDLD devices using this method, especially for DLD arrays with large quantities of nanoposts.

The geometry of DLD post arrays has a great effect on the separation characteristics of the array. Many studies have examined the effect of different post shapes on the critical diameter for particle separation or the ability to separate nonspherical, deformable particles.[5] Triangular posts with varying base-height ratios and vertex rounding have been explored, with triangular posts generally producing smaller (more favorable) ratios of gap spacing-to-critical diameter.[33,34] Diamond and airfoil-shaped posts have been shown to improve the DLD separation of soft particles, while minimizing device clogging.[35] Other post shapes that have been investigated include circular;[3] square;[5] polygonal with varying numbers of sides (including hexagonal and octagonal);[36,37] protrusion and groove structures such as I-, L-, and T-shaped posts;[16,37] and posts designed using optimization algorithms.[38] In these referenced studies, a combination of modeling and experimental approaches is used to characterize the DLD separation characteristics of new post geometries. Although many different post shapes have been explored, DLD research to date has been based on two types of post arrangements: parallelogram[5,16,24,37] (Figure 2a) and rotated-square[3,4,33,34] (Figure 2b). More variations of the basic repeating pattern have not been explored in the literature.

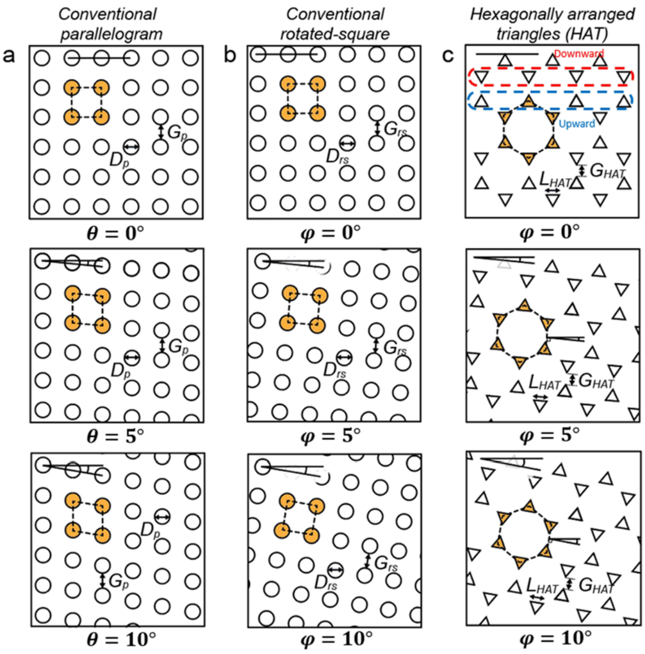

Figure 2. (a) Conventional parallelogram-type DLD array employing circular posts at three different array angles (θ). (b) Conventional rotated-square-type DLD array using circular posts at different structure angles (φ). (c) Bottom-up-inspired HAT geometry at various structure angles (φ). With triangular posts, a distinction is made between posts that face downward and those that face upward. Three different angles (0, 5, and 10°) are shown for each geometry. Note that no particle separation is expected to occur at 0° angle; the 0° configuration is shown as a comparison to illustrate the angles of rotation. Fluid flow is from left to right for all geometries.

In this work, we present a new DLD array geometry that we term "hexagonally arranged triangles" (HAT) (Figure 2c). The primary advantage of the HAT array geometry is the ability to fabricate this pattern using single-layer nanosphere lithography (NSL). NSL is a bottom-up fabrication approach that uses self-assembled nanospheres as a template to achieve nanoscale patterning over large surface areas.[39] In single-layer NSL, nanospheres self-assemble to form a hexagonally close-packed two-dimensional (2D) pattern. Any three spheres on the plane contain a void between them, which is approximately triangular in shape (Figure 1c). Unlike previous DLD studies using triangular-shaped posts, the triangles of the HAT array are rotated 60° relative to each other, following the void pattern produced by the templating nanospheres. Bottom-up self-assembly offers numerous advantages for nanoDLD compared to top-down nanofabrication, including lower-cost, higher-throughput nanoscale patterning without the need for expensive equipment.[40] Nanospheres can self-assemble into single-layer hexagonal close-packed arrays using a variety of simple, low-cost methods, such as spin-coating,[41] drop-casting,[42] or solvent evaporation.[43] With conventional single-layer NSL, the 2D self-assembled spheres can be used to form a mask for subsequent deposition (Figure 1d) of metal,[39] organic,[44] or oxide materials,[45] producing a HAT array upon the removal of the templating spheres (Figure 1e). The triangular posts produced by NSL can be easily scaled to various sizes, depending on the diameter of the templating spheres.[39] NSL has been shown to produce highly uniform patterns over large areas with minimal defects (>1 m^2).[46] Other patterns may also be produced with more complex variations of this approach.[47,48]

The goal of this work is to determine the feasibility of DLD separation using the HAT geometry and characterize the critical diameter vs structure angle relationship for this new array pattern. Finite element simulations of HAT arrays are used to provide theoretical evidence for DLD separation. A characteristic equation relating the array angle, gap spacing, and critical diameter is derived based on simulations and is expressed in a similar form to that of conventional DLD arrays. Theoretical results are validated using microscale DLD devices fabricated by two-photon direct laser write (DLW) three-dimensional (3D) printing to obtain a negative master mold using our previously reported method.[49] This approach ensures that experimental results for the HAT geometry provide accurate evaluation of the separation performance of the array pattern, without introducing complicating factors that may arise from bottom-up patterning defects and nanoscale effects. Potential complicating effects include array defects arising from nanosphere self-assembly, nonvertical post sidewalls, and misalignment of the enclosing microfluidic device with respect to the HAT pattern. Following this first-time validation of the DLD phenomenon using HAT arrays, future work may proceed to explore bottom-up fabrication of nanoDLD arrays with confidence that this unique array geometry is feasible for size-based particle separation.

■ MATERIALS AND METHODS

HAT Geometry. Triangular post position, diameter, and gap spacing for the HAT geometry are based on atomic force microscopy (AFM) images of single-layer NSL arrays fabricated by Hulteen and Van Duyne using 264 nm diameter nanospheres and Ag metal lift-off[39] (Supporting Information, Figure S1a). In both finite element simulations and experimental tests, single-layer NSL-inspired posts are approximated as equilateral triangles with perfectly straight sidewalls. Four simulations were conducted with varying combinations of post side length (L_{HAT}) and gap spacing (G_{HAT}) to demonstrate the consistency of separation at micro- and nanoscales and in the two cases of $L_{HAT} = G_{HAT}$ and $L_{HAT} \neq G_{HAT}$. Dimensions used in the four simulations were (i) $L_{HAT} = G_{HAT} = 141.5$ nm (based on the templating sphere radius of 264 nm), (ii) $L_{HAT} = 15.2$ μm, $G_{HAT} = 7.5$ μm (experimentally verified) (Supporting Information Figure S1b), (iii) $L_{HAT} = G_{HAT} = 15.2$ μm, and (iv) $L_{HAT} = G_{HAT} = 7.5$ μm. Simulation results presented are specifically based on $L_{HAT} = G_{HAT} = 15.2$ μm. Identical results were verified in COMSOL for all four simulation geometries.

Finite Element Simulations. COMSOL Multiphysics finite element software was used in the theoretical analysis of DLD separation with HAT arrays. A steady-state solver was set up in a 2D domain using the fluid-flow module that solves the Navier−Stokes equation under incompressible flow conditions. No slip condition was specified at the boundaries and post walls. For the microscale simulations, the designs were modeled in a 24 μm × 10 μm channel. The geometry was directly constructed within the COMSOL environment, and a fine mesh was used to compute the solution. A mesh independence test was conducted on the velocity profile to verify the simulation accuracy, with results provided in the Supporting Information, Figure S2.

Visualization of the DLD separation was performed through COMSOL's particle tracing module. The module treats particles as point masses, so "dummy walls" surrounding the actual posts with offset equal to the particle radius were generated to account for particle-post interactions. Particle-post interactions were modeled as elastic collisions using the bounce condition on the post boundary. Diffusion effects were not considered, and the flow profiles are assumed to not be altered by the presence of particles. Particle tracing simulations were validated by modeling circular posts in parallelogram arrangement and obtaining results that match published DLD experimental results (Supporting Information, Figure S3).[3]

Critical Diameter Analysis. The theoretical determination of the critical diameter using COMSOL Multiphysics was performed in two stages. First, a streamline analysis under steady-state conditions was used to identify the stall line which divides a flow stream into two parts (Figure 3a−c). Streamline analysis was conducted with a resolution of 100 equidistant streamlines between two posts. By tracking the location where the streamline splits at the next staggered post location, the critical diameter was approximated as 2× the distance from the edge of the post to the split streamline. In all cases, the streamline used for critical diameter estimation was the displacement-mode trajectory (i.e., the line that goes below the staggered post), leading to an overestimate of the critical diameter. Error bars in Figure 7 correspond to a 1% error in the critical diameter estimate introduced by the 100-streamline resolution. The error bars are asymmetrical because of the overestimate of the critical diameter. Second, to confirm the critical diameter estimate from the streamline analysis, the particle tracing module was implemented as described above to visualize particle trajectories with $D > D_c$ and $D < D_c$. Two sets of dummy walls corresponding to particle sizes up to ±10% of the critical diameter were generated in a single model. Particles with sizes corresponding to the dummy walls were introduced and resulted in size-based separation at the end of the channel (Figure 6). A MATLAB script was used to fit critical diameter vs structure angle results to the general form of the critical diameter expression[50] for the HAT array geometries. The fitting was performed with a resolution of four decimal places and a maximum error of 1.5% (Figure 7).

Microfluidic Device Fabrication. We created proof-of-concept DLD devices for both the conventional DLD and HAT DLD to test their particle sorting abilities. The proof-of-concept DLD devices were fabricated using DLW to print a negative master mold and replicating the pattern with polydimethylsiloxane (PDMS). Because of size limitations dictated by the fabrication approach, our proof-of-concept devices are in the microscale range.

The negative master molds were designed using the computer-aided drafting (CAD) program SolidWorks (Dassault Systèmes, France). The CAD files were then converted to the STL file format and imported into the computer-aided manufacturing (CAM) software DeScribe (Nanoscribe GmbH & Co. KG, Germany) to generate the laser path for the DLW process. For all the molds, the layer height and hatching parameters were 2.5 μm and 500 nm, respectively. The molds were printed on silicon substrates (25 mm × 25 mm) prepared by successive washes of acetone and isopropyl alcohol (IPA) before being dried with inert N_2 gas. The slides then underwent a 30 min oxygen plasma cleaning process before being silanized in a solution of 1 mM 3-(trimethoxysilyl) propyl methacrylate in toluene. The photoresist, IP-Q

Table 1. Comparison of Bottom-Up-Inspired HAT Array vs Conventional Parallelogram and Rotated-Square DLD Arrays

design type	post shape	post arrangement	post size and gap	angle
conventional DLD (parallelogram)	any	staggered arrays	independent	array
conventional DLD (rotated-square)	any	fixed square	independent	structure
HAT (single-layer NSL)	triangular	“upward” and “downward” facing triangles	dependent	structure

(Nanoscribe), was placed on the silicon substrate, and the slides were loaded into the Nanoscribe Photonic Professional GT DLW system. The molds were printed using the 10× objective lens in the DiLL mode configuration. The mold covered a large print area, approximately 12 mm × 3 mm. To cover this print area, the mold was printed using a stitching methodology to print the mold in 850 μm × 850 μm connected blocks. Each mold contained an 800 μm × 5000 μm DLD network and areas for two inlet ports and an outlet port. Following the DLW printing process, the molds were developed by rinsing in propylene glycol methyl ether acetate (PGMEA) bath for 30 min, followed by a 2 min IPA rinse to remove undeveloped photoresist.

To create the fluidically sealed PDMS device, liquid PDMS at a 10-to-1 ratio of base-to-curing agent was poured over the negative molds. The PDMS was cured at 50 °C for 3 h and then left at room temperature to complete the curing. Then, the PDMS was removed from the mold and ports were added at the inlets and outlet. To complete the device the PDMS was bonded to a glass substrate (30 mm coverslip, Bioptechs, Butler, PA) using an oxygen plasma bonding process.

Microfluidic Device Testing. Microfluidic testing was performed using the Fluigent Flow EZ system (Fluigent, France). Two solutions/suspensions were prepared for the microfluidic testing: (i) a buffer solution of deionized (DI) water and 3% (v/v) Tween 20 (MilliporeSigma, St. Louis, USA), and (ii) a nanoparticle suspension of DI water, 3% (v/v) Tween 20, 2.5% (v/v) 4.9 μm green, fluorescent polystyrene particles (Thermo Fisher Scientific, Waltham, USA), and 1.25% (v/v) 860 nm red, fluorescent polystyrene particles (Thermo Fisher Scientific, Waltham, USA). Flow rates in the channel were maintained in the 2−4 μL/min range. The fluid solutions were input into the DLD devices using fluorinated ethylene propylene tubing (Cole-Parmer, Vernon Hills, IL) and stainless-steel couplers (20 ga., Instech, Plymouth Meeting, PA). Fluorescence results were obtained using an inverted fluorescence microscope (Axio Observer.Z1, Zeiss, Germany) connected to a charge-coupled device (CCD) camera (Axiocam 503 Mono, Zeiss). Fluorescence images were analyzed using ImageJ (NIH, Bethesda MD) to determine the location of the particle streams in the DLD arrays. The position of the particle streams was found by locating the peak intensities at the entrance and the exit of the DLD arrays. The results are presented as mean ± standard deviation.

■ RESULTS AND DISCUSSION

Bottom-Up-Inspired HAT Geometry. The bottom-up-inspired HAT DLD geometry presents several unique features in terms of post positioning relative to the fluid-flow stream. To date, DLD post size and gap spacing are treated as independent parameters because of the conventional top-down approach used in the fabrication of DLD devices. However, when fabricated by NSL, the post size and gap spacing are equal and have a fixed relationship that depends on the size of the templating nanospheres used to produce these patterns.[39] The patterning produces six equilateral triangular posts surrounding each templating sphere, each equidistant from one another pointing outward from the center of the templating sphere. The post side length (L_{HAT}) and gap space (G_{HAT}) are equal by default, and their relationship with the templating sphere radius (r) is given by eq 1 (see derivation in the Supporting Information):

$$L_{\mathrm{HAT}} = G_{\mathrm{HAT}} = (4 - 2\sqrt{3})r \tag{1}$$

Using techniques such as reactive ion etching of the templating spheres, the size of the post can be reduced and the gap space enlarged, allowing additional control on the final dimensions of the HAT array.[47,51]

While the templating nanospheres produce six orientations of equilateral triangles, in the discussion pertaining to the DLD mechanism, there are two triangle orientations of significance to flow separation because of the symmetry of each “row” of posts. These two types of triangular posts will be called “upward”- and “downward”-facing posts (Figure 2c). This is in contrast to a conventional DLD geometry, where all the posts are oriented in the same direction. Additionally, as HAT posts present a fixed orientation relative to one another, changing the angle of the array relative to fluid flow requires rotating the entire bottom-up-templated structure. This is different from parallelogram-type DLD arrays (Figure 2a), but comparable to the rotated-square DLD array design (Figure 2b).[3] The angle of rotation of HAT DLD arrays will be referred to as the “structure angle (φ),” which is comparable to the “array angle (θ)” in conventional parallelogram-type DLD arrays. Figure 2 illustrates the concept of the structure angle applied to the HAT array pattern considered in this work (Figure 2c) and compares it at three different angles (0, 5, and 10°). Table 1 summarizes these features of HAT arrays compared to the conventional parallelogram and rotated-square DLD arrays.

Finite Element Simulations of the HAT Geometry. Figure 3 illustrates the streamline approach used to verify DLD separation and estimate the critical diameter for particle separation with the HAT geometry. Simulation results presented in Figure 3a−c are for a 10° structure angle; streamline analysis was also conducted for structure angles ranging from 3 to 15°, with the critical diameter results summarized in Figure 7. The streamline that terminates on the post surface, known as the stall line, lies in the region where the streamlines are more dense (Figure 3a). The deterministic separation effects of the HAT geometry are clearly seen by contrasting the streamlines above and below a separating post (indicated in yellow in Figure 3b−c). Representative circular particles with diameters less than and greater than the critical diameter are shown in Figure 3b,c, respectively, to illustrate the separation mechanism. Particles with size less than the critical diameter ($D < D_c$) move in a zig-zag pattern, maintaining their original trajectory, as shown by the red sphere (Figure 3b). Particles with the size larger than the critical diameter ($D > D_c$) undergo lateral displacement at each successive post, leading to size-based separation (Figure 3c). The separation of particles smaller and larger than the critical diameter is predicted for the HAT geometry using streamline analysis, theoretically

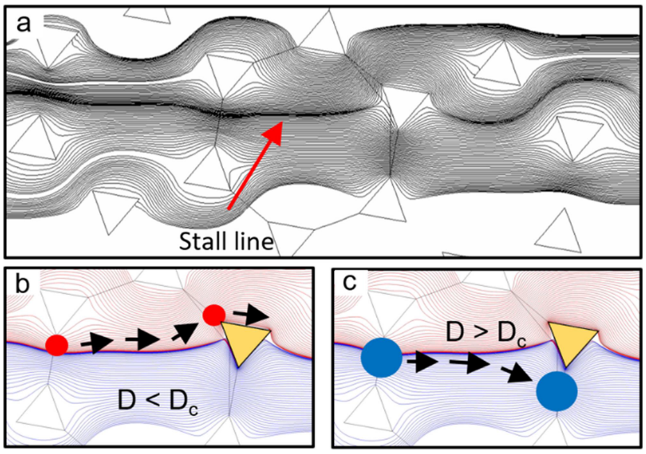

Figure 3. Streamline analysis for the HAT geometry. (a) Streamlines above and below a post of interest. The region where the lines are more closely spaced corresponds to the stall line. (b) Particle trajectory for a particle diameter smaller than the critical diameter ($D < D_c$). (c) Particle trajectory for a particle diameter larger than the critical diameter ($D > D_c$).

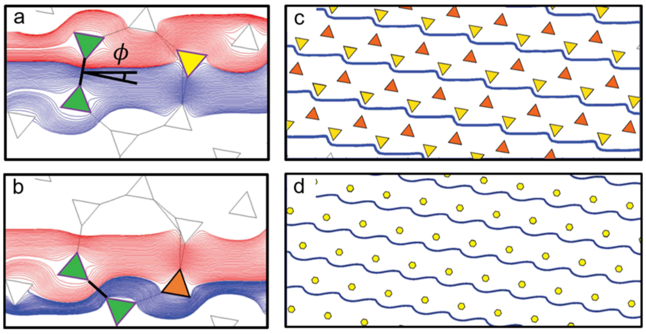

Figure 4. Flow profiles at the two different post types for HAT arrays. (a) Stall line extending upstream from a downward-facing post (yellow) passes between a set of posts (green pair) that are perpendicular to the structure angle. (b) Stall line extending upstream from an upward-facing post (orange) passes through a set of posts that are not perpendicular to the structure angle. (c) In HAT arrays, only rows containing downward-facing posts (yellow) contribute to lateral displacement, while upward-facing post rows do not cause separation. (d) Every row in a conventional DLD array contributes to "bump" mode lateral displacement causing separation.

validating the feasibility of this array configuration for DLD separation.

An interesting phenomenon arises when comparing the separation characteristics of "upward-" vs "downward-" facing triangular posts (Figure 4). Stall lines that terminate on a downward-facing triangular post (indicated in yellow in Figure 4a) pass between posts that are perpendicular to the structure angle φ and have critical diameters that are physically realizable. In contrast, stall lines that end on an upward-facing triangular post pass through posts that are not aligned perpendicular to the structure angle φ (Figure 4b). The distance from the stall line to the edge of these posts results in a critical diameter that is greater than the gap space available, thereby resulting in no actual separation at upward-facing triangular posts. This results in two types of post rows in the HAT geometry, one where particle sorting is possible (downward) and the other where sorting does not take place (upward) (Figure 4c).

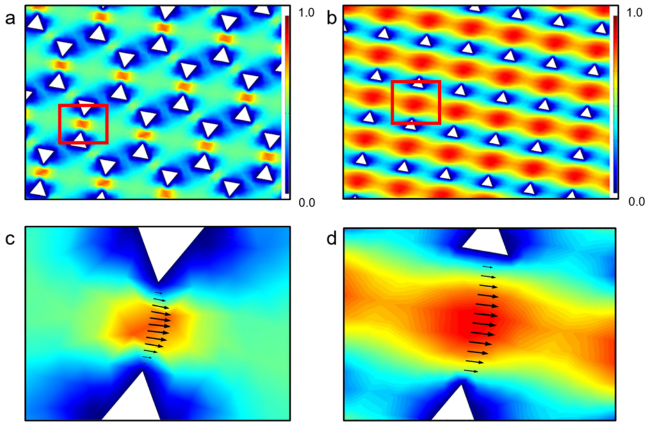

Figure 5. Simulated velocity profiles for (a) HAT and (b) conventional DLD with triangular posts. (c) Zoomed-in view of the symmetric flow profile between the two triangular posts in the HAT geometry. (d) Zoomed-in view of the asymmetric flow profile between posts for conventional DLD arrays with triangular-shaped posts. Both geometries are simulated at a structure/array angle of 10° relative to the flow stream. Fluid flow is from left to right.

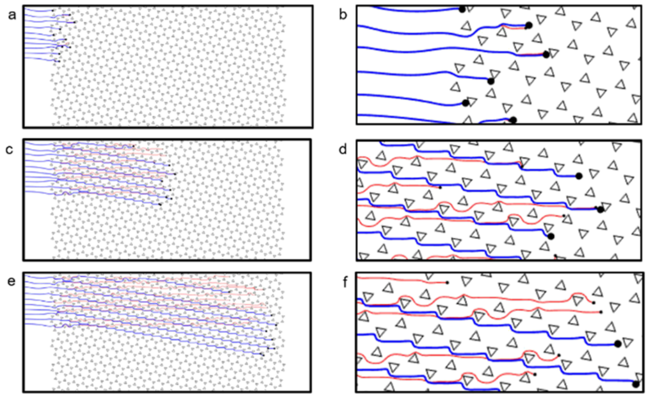

Figure 6. Particle tracing simulation showing particle separation for HAT arrays. Snapshots are taken at three different times showing particles (a) just after entering, (c) reaching mid-way, and (e) exiting the channel. (b), (d), (f) Zoomed-in views of particles along each of the corresponding sections of the channel showing the separation process.

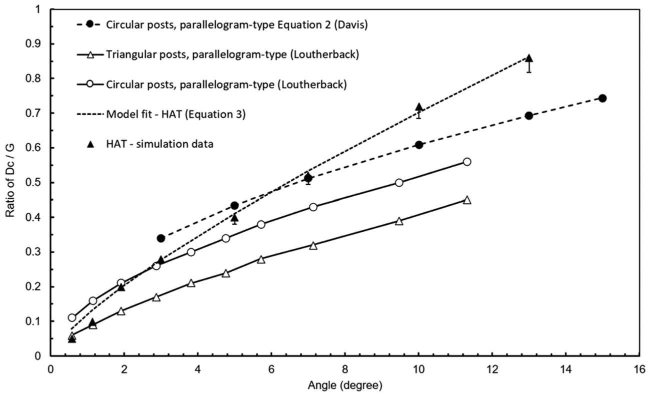

Figure 7. Comparison of normalized critical diameter vs array/structure angle relationships for parallelogram-type DLD arrays with circular posts (eq 2 and Loutherback et al.[34]), parallelogram-type DLD arrays with triangular posts (Loutherback et al.[34]), and HAT geometry (finite element simulations, eq 3).

A comparison of particle flow in Figure 4c,d illustrates the difference in lateral separation between a conventional DLD array (Figure 4d) and an HAT array (Figure 4c). Because of the singular type of post present in a conventional DLD array (irrespective of the post shape), the streamline distribution between any two posts is representative of the entire array. This leads to separation taking place across every post, and by extension, along every array row (Figure 4d). Owing to the two distinct flow profiles induced by upward- and downward-facing triangular posts in the HAT array, particle separation takes place along alternating rows in the HAT geometry (Figure 4c). In Figure 4c, the structure angle is directed downward, and the fluid moves from the left to the right in the channel. The rows that have posts pointing downward (yellow), that is, in the direction where the structure angle induces lateral displacement cause “bump” mode travel for particles with $D > D_c$. The rows containing posts pointed in the opposite “upward” direction (orange) cause no particle separation.

Figure 5 compares velocity profiles for HAT arrays (Figure 5a,c) to conventional DLD arrays consisting of triangular posts (Figure 5b,d). With the HAT geometry, we observe that there are differences in flow velocities among gaps oriented perpendicular to structure angle φ (zones with high velocity flow, where particle separation takes place) vs gaps that are not perpendicular to the structure angle (zones with low velocity flow where particle separation does not take place) (Figure 5a). Figure 5c provides a zoomed-in view of the symmetric flow profile arising between the points of two adjacent triangles oriented perpendicular to the structure angle. With conventional DLD using triangular post arrays, the flow profile between adjacent rows of triangular posts is asymmetric because of the fact that the bottom edge of one triangle faces the vertex of the adjacent triangle (Figure 5b,d).[5,34] Vernekar et al. found that the presence of highly asymmetric post shapes and unequal gap spacings between posts is associated with increased anisotropic permeability in DLD arrays.[4] They also showed that a rotated-square type DLD configuration is preferable to parallelogram-type to reduce anisotropy effects. It is noteworthy that the post-gap asymmetry present in parallelogram-type triangular DLD post arrays does not arise with the HAT geometry, as all gap spaces are symmetric. On the other hand, the presence of multiple triangle orientations in the channel with the HAT geometry is likely to increase anisotropy in the array. Using pressure simulations in COMSOL, we estimate anisotropy (A) values for HAT arrays to be in the range of 0.05−0.09, with the range arising based on the location of pressure measurement relative to the triangle posts. HAT anisotropy exceeds that reported for equilateral triangles in the rotated-square arrangement (A = 0.032),[4] is comparable to that of circular posts in a parallelogram arrangement (A = 0.06),[4] and is lower than that of right triangles in the rotated-square arrangement (A = 0.18).[4]

Figure 6 provides particle tracing simulation results for HAT arrays captured near the start (Figure 6a,b), mid-point (Figure 6c,d), and end (Figure 6e,f) of the channel. The presented results are for a structure angle of 10°. A clear separation of particles with $D < D_c$ (red traces) and $D > D_c$ (blue traces) is observed, confirming the streamline analysis results of Figure 3. Particle tracing simulations also confirm previous observations that the displacement-mode trajectory for particles is only observed when larger particles move between post pairs that are aligned perpendicular to the structure angle, φ (Figure 4c). With the exception of particle trajectories near the channel entrance and wall, particles with $D > D_c$ undergo lateral displacement exclusively along rows of posts facing the downward direction.

Along the walls of the channel, the posts are either fully present, partially present, or completely absent. This can result in particle flow regimes different from the bulk flow, which has been explored for conventional DLD designs in previous work.[52] Similarly, for the starting few post columns, the flow regime is not fully developed into uniformly split streamlines, causing deviations in particle trajectories from the ideal, predicted DLD flow paths present in the central bulk of the channel. Within the range of structure angles (3−15°) studied for the HAT geometry, it was found that deviations can occur up to three post columns into the channel from the start of the post region, and up to two post rows into the channel from the channel walls.

In conventional DLD microfluidic devices (parallelogram or rotated-square arrays), the critical diameter for particle separation is directly proportional to the gap spacing. Finite element simulations of HAT arrays using three different values of gap spacing (141.5 nm, 15.2 μm, and 7.5 μm) indicate that this same proportionality holds true for the HAT geometry. For a parallelogram DLD device with circular posts, the relationship between the critical diameter for particle separation, D_c, and the design variables G and θ have been determined empirically by Davis as (eq 2):[50]

$$D_c = 1.4G(\tan\theta)^{0.48} \tag{2}$$

Theoretically determined D_c values for the HAT geometry simulated at 0.57, 1.14, 1.9, 3, 5, 7, 10, and 13° structure angles were fit to a general form of eq 2, using structure angle φ in place of θ (eq 3):

$$D_c = 2.63G(\tan\varphi)^{0.76} \tag{3}$$

The results are plotted in Figure 7, with eq 3 plotted as a dashed line connecting the simulated array angle data points.

Figure 7 compares the predicted separation characteristics of HAT arrays with published values for parallelogram-type DLD arrays, including (1) eq 2 empirical fit for circular posts,[50] (2) data from Loutherback et al. for circular posts,[34] and (3) data from Loutherback et al. for triangular posts.[34] D_c values are normalized by the gap spacing, G, for each DLD design. Critical diameter results in Figure 7 are plotted until the maximum theoretical angle is reached. The maximum theoretical angle is reached when the critical diameter determined by the simulations becomes equal to the gap space between the posts such that particles would not be able to pass through the array.

Results for the HAT geometry indicate a steeper increase in the critical diameter with increasing structure angle compared to parallelogram-type DLD arrays with circular and triangular posts. The HAT array achieves excellent separation characteristics at low structure angles (<7°), outperforming empirical results for the common parallelogram-type circular post arrays described using eq 2 and closely matching results for the circular post arrays reported by Loutherback et al. It is known that simulation estimates for the critical diameter are typically lower than experimental values,[14] which may explain the discrepancy between eq 2 (experimental results of Davis) and the results of Loutherback et al. (combined simulation and experiments) (Figure 7). At structure angles >7°, the predicted critical diameter for the HAT array exceeds that of parallelo-

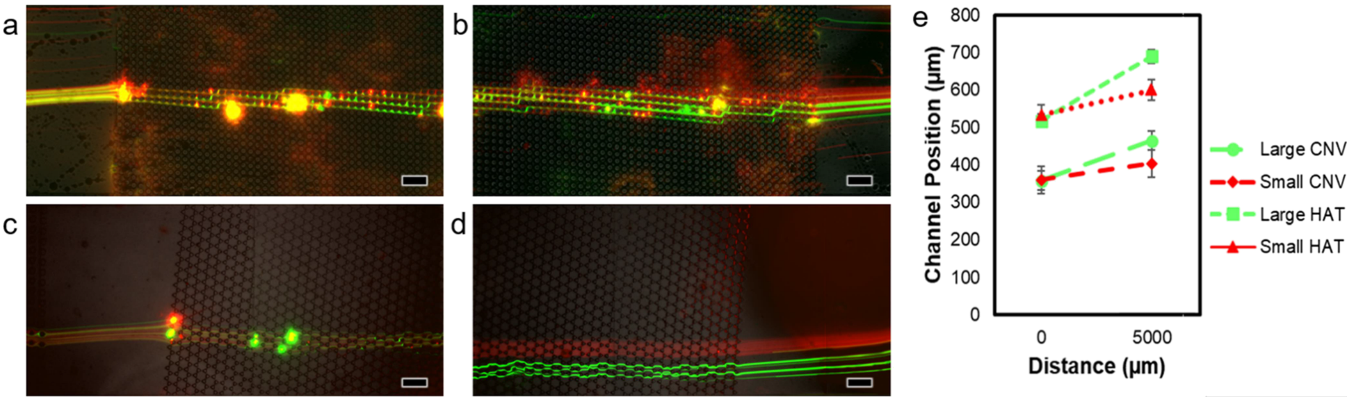

Figure 8. Particle stream testing for the conventional DLD array: (a) Inlet showing red (small) and green (large) particles combined at the start of the 5000 μm channel. (b) Outlet showing the particles separated. Particle stream testing for the HAT array: (c) Inlet showing red (small) and green (large) particles combined. (d) Outlet showing particles separated into two different streams. Scale bars = 100 μm. (e) Particle stream position determined by fluorescence image analysis. The larger particles have a larger shift than smaller particles in both the conventional (CNV) and HAT DLD arrays.

gram arrays with circular posts. The HAT geometry also has a smaller range of theoretically allowable structure angles compared to conventional DLD arrays: above 14°, the critical diameter for particle separation with HAT exceeds 90% of the available gap space. The maximum theoretical structure angle for HAT is 15.65° (Figure 7). As with any DLD design, there is a tradeoff between the benefits of reducing the structure angle and the resulting increase in the channel length required to achieve the same lateral separation. While the critical diameter for the separation of the HAT geometry exceeds that reported by Loutherback et al. for parallelogram-type arrays with triangular posts, we note that the HAT geometry avoids issues with flow asymmetry between gaps, reducing anisotropic permeability in DLD arrays.[4]

Experimental Results of DLD Separation. To evaluate the ability of the DLD arrays to separate different-sized particles, we performed continuous-flow microfluidic experiments with different-sized fluorescent polystyrene microparticles (red 860 nm diameter and green 4.9 μm diameter) and monitored the particle streams under fluorescence microscopy. We input a buffer solution to both sides of the DLD array near the side walls to focus the flow of the particle stream to the center of the DLD array, reducing the particle-side wall interactions (i.e., boundary effects) that can disrupt the DLD behavior.[53] The fabricated conventional and HAT DLD arrays have an equal gap size of 11 μm, leading to critical diameters of 4.66 and 3.29 μm, respectively. The array angles are 5.2 and 5.0° for the conventional and HAT arrays, respectively. The critical diameters for both DLD arrays are less than the diameter of the larger (green) microparticles and greater than the smaller (red) particles. Therefore, the green particles are laterally displaced by the DLD array, separating the larger particles from the smaller particles (Figure 8a−d). At the beginning of the conventional and HAT DLD arrays (Figure 8a,c), the small and large particles are mixed, creating a single stream. After 5000 μm, both the conventional and HAT arrays caused the larger (green) particles to laterally displace, creating their own streamline, as shown in Figure 8b,d, respectively. While the smaller particles at the outlet (Figure 8d) have a perfectly straight net path through the zig-zag mode, at the inlet because of overlap and mild clogging, it is difficult to determine if there is any lateral displacement of smaller particles (Figure 8c). Despite this, there is a clear separation between the two streams at the channel end, achieving the objective of size-based particle sorting. These results were also verified numerically through image analysis. The conventional DLD array had peak shifts of 43.9 ± 36.2 and 106 ± 25.9 μm, corresponding to the small and large particles (Figure 8e). The shift was more pronounced in the HAT DLD array with peak shifts of 66.9 ± 21.3 μm for the small particles and 173 ± 18.3 μm for the large particles, as shown in Figure 8e.

■ CONCLUSIONS

Theoretical analysis of the HAT array geometry indicates the potential for deterministic particle separation using nanopost arrays fabricated by single-layer NSL bottom-up patterning. Despite several unique characteristics, including rotated triangle posts and gap spacing/post size dependencies when templated by single-layer NSL, the geometry demonstrates the essential qualities of a DLD array, namely, (1) deterministic particle separation based on size and (2) dependence of D_c/G on the array/structure angle. Experimental validation at the microscale confirms the DLD separation characteristics of the HAT array geometry. In addition to the fabrication advantages of a bottom-up nanopost array pattern, the HAT array outperforms conventional DLD arrays based on circular posts for array/structure angles <7° (as described by eq 2) and avoids the asymmetric flow profile effects of parallelogram-type DLD arrays with triangular posts.

Further study is needed to examine particle separation with the HAT geometry at the nanoscale and using arrays fabricated by single-layer NSL. In particular, diffusion effects arising in the low Peclet number ($Pe < 20$)[12] regime should be explored for nanoDLD with HAT. While DLD arrays have the benefit of repeated separation motion providing robustness to array defects, the effect of randomized bottom-up fabrication errors on the separation efficiency must also be examined. These studies may proceed knowing that the theoretical basis for bottom-up-inspired array geometries is in place, and motivated by the potential for rapid, low-cost fabrication of sub-100 nm DLD devices.

Finally, we briefly describe a possible fabrication approach for DLD devices using NSL. Templating nanospheres are first self-assembled on a silicon wafer. The HAT array pattern is obtained *via* metal deposition and nanosphere lift-off. A photolithography step is used to pattern the flow channel at the desired structure angle (φ). Nanoscale HAT posts and the microscale flow channel are then etched into the silicon substrate and bonded to a glass slide to seal the channel.

■ ASSOCIATED CONTENT

Supporting Information

The Supporting Information is available free of charge at https://pubs.acs.org/doi/10.1021/acs.analchem.1c03035.

> Derivation of HAT arrays inspired from the bottom-up, single-layer (NSL) pattern; COMSOL mesh independence results; COMSOL mesh convergence parameters; validation of the model through simulations of conventional circular-post DLD array separation; and derivation of HAT array dimensions (PDF)

■ AUTHOR INFORMATION

Corresponding Author

Roseanne Warren – *Department of Mechanical Engineering, University of Utah, Salt Lake City, Utah 84112, United States*; orcid.org/0000-0002-0520-8906;
Email: roseanne.warren@utah.edu

Authors

Talha M. Razaulla – *Department of Mechanical Engineering, University of Utah, Salt Lake City, Utah 84112, United States*; orcid.org/0000-0002-4808-2194
Olivia M. Young – *Department of Mechanical Engineering, University of Maryland, College Park, Maryland 20742, United States*
Abdullah Alsharhan – *Department of Mechanical Engineering, University of Maryland, College Park, Maryland 20742, United States*
Ryan D. Sochol – *Department of Mechanical Engineering, University of Maryland, College Park, Maryland 20742, United States*

Complete contact information is available at:
https://pubs.acs.org/10.1021/acs.analchem.1c03035

Author Contributions

R.W. and R.D.S conceived the project and acquired funding. T.R. ran simulations and wrote the original draft. O.M.Y. and A.A. conducted experiments and added to the manuscript. All authors modified the manuscript and contributed equally to modifications.

Notes

The authors declare no competing financial interest.

■ ACKNOWLEDGMENTS

This work was supported in part by the U.S. National Science Foundation (NSF) Award #1761273 and #1761395.

■ REFERENCES

(1) Gossett, D. R.; Weaver, W. M.; Mach, A. J.; et al. *Anal. Bioanal. Chem.* **2010**, *397*, 3249−3267.

(2) El-Ali, J.; Sorger, P. K.; Jensen, K. F. *Nature* **2006**, *442*, 403−411.

(3) Huang, L. R.; Cox, E. C.; Austin, R. H.; Sturm, J. C. *Science* **2004**, *304*, 987−990.

(4) Vernekar, R.; Krüger, T.; Loutherback, K.; Morton, K.; Inglis, D. W. *Lab Chip* **2017**, *17*, 3318−3330.

(5) Zhang, Z.; Henry, E.; Gompper, G.; Fedosov, D. A. *J. Chem. Phys.* **2015**, *143*, 243145.

(6) Kulrattanarak, T.; van der Sman, R. G. M.; Lubbersen, Y. S.; et al. *J. Colloid Interface Sci.* **2011**, *354*, 7−14.

(7) Collins, D. J.; Alan, T.; Neild, A. *Lab Chip* **2014**, *14*, 1595−1603.

(8) Chang, S.; Cho, Y.-H. *Lab Chip* **2008**, *8*, 1930.

(9) Chen, X.; Ren, Y.; Liu, W.; et al. *Anal. Chem.* **2017**, *89*, 9583−9592.

(10) Devendra, R.; Drazer, G. *Anal. Chem.* **2012**, *84*, 10621−10627.

(11) Zhang, T.; Hong, Z.-Y.; Tang, S.-Y.; et al. *Lab Chip* **2020**, *20*, 35−53.

(12) Heller, M.; Bruus, H. *J. Micromech. Microeng.* **2008**, *18*, No. 075030.

(13) Zeming, K. K.; Thakor, N. V.; Zhang, Y.; Chen, C.-H. *Lab Chip* **2016**, *16*, 75−85.

(14) Hochstetter, A. *Micromachines* **2020**, *11*, 468.

(15) Beech, J. P.; Holm, S. H.; Adolfsson, K.; Tegenfeldt, J. O. *Lab Chip* **2012**, *12*, 1048.

(16) Zeming, K. K.; Ranjan, S.; Zhang, Y. *Nat. Commun.* **2013**, *4*, 1625.

(17) Civin, C. I.; Ward, T.; Skelley, A. M.; Gandhi, K.; Peilun Lee, Z.; Dosier, C. R.; D'Silva, J. L.; Chen, Y.; Kim, M. J.; Moynihan, J.; Chen, X.; Aurich, L.; Gulnik, S.; Brittain, G. C.; Recktenwald, D. J.; Austin, R. H.; Sturm, J. C. *Cytometry A* **2016**, *89*, 1073−1083.

(18) Wang, G.; Crawford, K.; Turbyfield, C.; Lam, W.; Alexeev, A.; Sulchek, T. *Lab Chip* **2015**, *15*, 532−540.

(19) Holm, S. H.; Beech, J. P.; Barrett, M. P.; Tegenfeldt, J. O. *Anal. Methods* **2016**, *8*, 3291−3300.

(20) Tran, T. S. H.; Ho, B. D.; Beech, J. P.; Tegenfeldt, J. O. *Lab Chip* **2017**, *17*, 3592−3600.

(21) Inglis, D. W.; Morton, K. J.; Davis, J. A.; et al. *Lab Chip* **2008**, *8*, 925.

(22) Green, J. V.; Radisic, M.; Murthy, S. K. *Anal. Chem.* **2009**, *81*, 9178−9182.

(23) Morton, K. J.; Loutherback, K.; Inglis, D. W.; et al. *Lab Chip* **2008**, *8*, 1448.

(24) Joensson, H. N.; Uhlén, M.; Svahn, H. A. *Lab Chip* **2011**, *11*, 1305−1310.

(25) Tottori, N.; Hatsuzawa, T.; Nisisako, T. *RSC Adv.* **2017**, *7*, 35516−35524.

(26) Karabacak, N. M.; Spuhler, P. S.; Fachin, F.; et al. *Nat. Protoc.* **2014**, *9*, 694−710.

(27) Okano, H.; Konishi, T.; Suzuki, T.; Suzuki, T.; Ariyasu, S.; Aoki, S.; Abe, R.; Hayase, M. *Biomed. Microdevices* **2015**, *17*, 59.

(28) Liu, C.; Guo, J.; Tian, F.; et al. *ACS Nano* **2017**, *11*, 6968−6976.

(29) Wunsch, B. H.; Smith, J. T.; Gifford, S. M.; et al. *Nat. Nanotechnol.* **2016**, *11*, 936−940.

(30) Smith, J. T.; Wunsch, B. H.; Dogra, N.; et al. *Lab Chip* **2018**, *18*, 3913−3925.

(31) Wunsch, B. H.; Kim, S.-C.; Gifford, S. M.; et al. *Lab Chip* **2019**, *19*, 1567−1578.

(32) Kim, S.-C.; Wunsch, B. H.; Hu, H.; Smith, J. T.; Austin, R. H.; Stolovitzky, G. *Proc. Natl. Acad. Sci. U. S. A.* **2017**, *114*, 201706645.

(33) Loutherback, K.; Puchalla, J.; Austin, R. H.; Sturm, J. C. *Phys. Rev. Lett.* **2009**, *102*, No. 045301.

(34) Loutherback, K.; Chou, K. S.; Newman, J.; Puchalla, J.; Austin, R. H.; Sturm, J. C. *Microfluid. Nanofluid.* **2010**, *9*, 1143−1149.

(35) Al-Fandi, M.; Al-Rousan, M.; Jaradat, M. A. K.; Al-Ebbini, L. *Robot. Comput. Integr. Manuf.* **2011**, *27*, 237−244.

(36) Wei, J.; Song, H.; Shen, Z.; et al. *IEEE Trans. NanoBiosci.* **2015**, *14*, 660−667.

(37) Ranjan, S.; Zeming, K. K.; Jureen, R.; Fisher, D.; Zhang, Y. *Lab Chip* **2014**, *14*, 4250−4262.

(38) Hyun, J.; Hyun, J.; Wang, S.; Yang, S. *Sep. Purif. Technol.* **2017**, *172*, 258−267.

(39) Hulteen, J. C.; Van Duyne, R. P. *J. Vac. Sci. Technol. Vac. Surf. Films* **1995**, *13*, 1553−1558.

(40) Wang, Y.; Zhang, M.; Lai, Y.; Chi, L. *Nano Today* **2018**, *22*, 36−61.

(41) Bekeris, M.; Truong, T.; Carron, S.; Karimi, Z.; Feng, H.; Nze, U.; Beeman, M.; Sochol, R. D.; Warren, R. *Rapid Res. Lett.* **2020**, *14*, No. 2000328.
(42) Bognár, J.; Szűcs, J.; Dorkó, Z.; Horváth, V.; Gyurcsányi, R. E. *Adv. Funct. Mater.* **2013**, *23*, 4641−4641.
(43) Lazarov, G. S.; Denkov, N. D.; Velev, O. D.; Kralchevsky, P. A.; Nagayama, K. *J. Chem. Soc., Faraday Trans.* **1994**, *90*, 2077−2083.
(44) Nguyen, V.-Q.; Schaming, D.; Martin, P.; Lacroix, J.-C. *Langmuir* **2019**, *35*, 15071−15077.
(45) Kang, M.; Losego, M.; Sachet, E.; Maria, J.-P.; Franzen, S. *ACS Photonics* **2016**, *3*, 1993−1999.
(46) Gao, P.; He, J.; Zhou, S.; et al. *Nano Lett.* **2015**, *15*, 4591−4598.
(47) Kosiorek, A.; Kandulski, W.; Glaczynska, H.; Giersig, M. *Small* **2005**, *1*, 439−444.
(48) Luo, L.; Akinoglu, E. M.; Wu, L.; et al. *Nanotechnology* **2020**, *31*, 245302.
(49) Alsharhan, A. T.; Stair, A. J.; Acevedo, R.; Razaulla, T.; Warren, R.; Sochol, R. D. *J. Microelectromech. Syst.* **2020**, *29*, 906−911.
(50) Davis, J. A. *Microfluidic Separation of Blood Components through Deterministic Lateral Displacement*. PhD Dissertation, Princeton University, Princeton, NJ, 2008. http://citeseerx.ist.psu.edu/viewdoc/summary?doi=10.1.1.513.6416 (accessed 2021-07-09).
(51) Domonkos, M.; Demo, P.; Kromka, A. *Crystals* **2020**, *10*, 118.
(52) Pariset, E, Pudda, C, Boizot, F, Verplanck, N., Berthier, J., Thuaire, A., Agache, V. Particle Separation: Anticipating Cutoff Diameters in Deterministic Lateral Displacement (DLD) Microfluidic Devices for an Optimized Particle Separation (Small 37/2017). *Small* **2017**;*13*(). DOI: 10.1002/smll.201770201
(53) McGrath, J.; Jimenez, M.; Bridle, H. *Lab Chip* **2014**, *14*, 4139−4158.